International Journal of Adhesion and Adhesives xxx (xxxx) xxx–xxx

Contents lists available at ScienceDirect

International Journal of Adhesion and Adhesives

journal homepage: www.elsevier.com/locate/ijadhadh

Bonding performance after aging of fusion bonded hybrid joints

K. Lippky*, S. Hartwig, D. Blass, K. Dilger

Technische Universitaet Braunschweig, Institute of Joining and Welding, Langer Kamp 8, 38106 Braunschweig, Germany

ARTICLE INFO

Keywords:
Surface treatment
Aging
Hot-melt
Lap-shear

ABSTRACT

The investigations of this article are showing the bonding performance after aging of hybrid fusion bonds in combination with a laser pre-treatment. The investigated materials are a galvanized steel (HX340 LAD Z100MB) and two glass fiber reinforced Polyamide 6 materials. In order to achieve a structural strength of the fusion bond a laser pre-treatment is used. The investigation is focusing on the changes from the laser pre-treatment to the galvanized surface by analyzing the steel surface with a scanning electron microscope, energy disperse X-ray spectroscopy, micro sections and surface roughness measurements. The composition of the applied thermoplastic materials is not in the focus of the article which is why different manufacturers for the fiber reinforced thermoplastic material have been chosen. The aging of the samples is done by a climate change (PV1200) and a salt spray (PV1210) test in order to evaluate different aging mechanisms. Furthermore the investigation is providing a crucial finding by showing the impact of a batch change on the achievable lap-shear strength by comparing two batches from the same manufacturer. The results of the laser surface pre-treatment show that the zinc coating of the steel adherend is reduced significantly and does not provide a closed coating. The climate change test after 100 cycles showed no decrease of lap-shear strength compared to the reference when the highest investigated pre-treatment intensity is applied to the surface. The salt spray test showed a corrosion of the pre-treated area for laser pre-treatment settings which generate a low amount of oxygen on the surface. The pre-treatment settings generating a more oxidized surface (medium and high intensity) showed only a minor influence on the achievable lap-shear strength after 90 cycles.

1. Introduction and state of the art

The demand for lightweight structures especially in the automotive industry is increasing [1–3]. Due to the higher demand the production processes need to become more efficient. As recent investigations show the usage of fiber reinforced thermoplastics (FRTP) becomes more and more common in the automotive field [4–7]. One reason for this development is the fast production process which thermoplastic materials enable because of the missing curing times compared to thermosetting materials [8]. Furthermore the application of thermoplastic fiber reinforced materials enables the stocking of sheets which can be processed (e. g. shaped and bonded) in a subsequent process as it would be with steel sheets. This enables the decoupling of the production of a semi-finished part (thermoplastic fiber reinforced sheet) and the final shaping and joining [9–11]. Due to the high material costs of fiber reinforced materials the automotive industry is focusing on the application of these materials in combination with metals to hybrid parts [6,9] based on the dominating metals which are steel alloys with a zinc coating [12,13]. By combining thermoplastic fiber reinforced plastics with already applied steel alloys, an increased weight-specific performance (compared to a monolithic steel part) at lower costs (compared to a monolithic fiber reinforced part) can be achieved [10,14]. The production of a hybrid part is normally done by shaping the metal and the fiber reinforced thermoplastic material into a semi-finished part and combining them in a subsequent adhesive joining step. With the usage of thermoplastic fiber reinforced materials this process can be changed because these materials enable an integrated part production process which was for example introduced in [11]. By combining the processes of shaping and joining the overall cycle time can be reduced due to the missing application of an adhesive and the necessary curing time. In this production scenario the hybrid part is joined by using the fusion bonding technique as it was for example introduced by [15]. This technique is based on the fusion and consolidation of two thermoplastic fiber reinforced adherends to build a joint. Furthermore this technique can also be applied on different adherend combinations as long as one of them is a thermoplastic material, as several investigations have shown over the past [16–18].

Fusion bonding therefor can be applied in a variety of applications. The investigations carried out over the past can be structured by the applied heating technique which is necessary to fuse the thermoplastic

* Corresponding author.
E-mail address: k.lippky@tu-braunschweig.de (K. Lippky).

https://doi.org/10.1016/j.ijadhadh.2019.01.025

material and the applied surface pre-treatment to increase the overall joint performance. The most promising heating techniques are among others the hot-tool resp. hot-plate [19,20], the laser (in a conductive or transmission setup) [21–24], the friction [25,26] and the inductive heating [16,27]. All introduced heating techniques apply heat to a metal part to conductively heat the thermoplastic part above its melting temperature. The heating techniques should be more or less interchangeable concerning the necessities of the desired process because the joint is created mostly in the same way, by pressing a hot metal part onto the fiber reinforced thermoplastic (FRTP) material. In order to achieve sufficient joint strength with a fusion bonded hybrid joint investigations showed that a pre-treatment is inevitable but again different pre-treatment strategies can be used in order to achieve the desired joint strength. [16,17,19,28–30] Most of the investigated pre-treatment strategies are well known from adhesive bonding of thermoplastic materials and metals as the pre-treatment with plasma, sand blasting, adhesion promoters [31] and laser pre-treatments [21–24,28,29,32]. In another investigation by the author a laser pre-treatment showed promising results to reach a structural strength for the investigated combination of steel (DC01) and fiber reinforced Polyamide 6 [33]. Furthermore, the laser showed good results for also cleaning metal surfaces from contaminations like deep drawing oils, which are necessary for shaping a metal part. [34].

The pre-treatment of a metal part by laser leads to a change of surface topography [35]. These changes are based on the interaction between the laser beam and the surface as shown in Fig. 1. The laser beam generates a liquid melt layer and a vapor which forces the molten material out of the interaction area. This creates a crater like structure by overlapping the laser pulses or laser interaction areas the formed crater edges are remolten and a more or less continuous melting bath is generated which forms a new surface topography [35,36]. This effect can be used to form discrete lines on the surfaces as done by [37]. In order to structure surfaces completely to achieve for example a cleaning additionally to a structuring the overlapping of lines is necessary as done by [35].

The goal of a suchlike surface pre-treatment is to generate defined or undefined undercuts in order to increase the possibilities for a mechanical interlocking of the later applied thermoplastic material. But additionally to the change of the macroscopic surface structure a change of surface chemistry has been observed which leads to the formation of submicroscopic structures as the investigations of [38] showed on $AlMg_3$ or on low carbon steel [39] surfaces. By using a transmission electron microscope [38] showed that an oxide layer forms during the laser pre-treatment of an aluminum surface. This oxide layer enables an adhesive the infiltration of the metal adherend as proposed by [38]. The findings of an oxide layer generated by a laser pre-treatment are also observed by [40]. The changes in the surface topography on a macroscopic, microscopic and submicroscopic scale lead to an increase of surface area as the investigations of [40] showed. This investigation used the Brunauer-Emmet-Teller theory [41] to determine the increase of surface area after the application of a laser pre-treatment (with a wavelength of 1064 nm) to an AlMgSi1 which increased the surface area by up to 247 times compared to the initial state. The changes made to metal surfaces therefor result in a change of topography and surface chemistry as the building of oxide layers observed by [38,40] showed on aluminum.

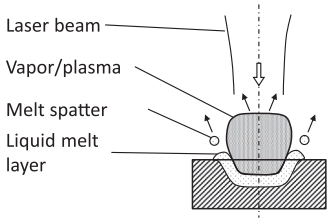

Fig. 1. Schematic interaction of a laser beam with a metal surface based on [36].

The interaction of a metal surface and a Polyamide 6 has been investigated by [42]. The results show that the adhesion forces between a metal surface and a Polyamide 6 are based on polar and disperse forces. By increasing the amount of oxides on the metal surfaces more polar or hydrogen bonds can be formed with the amide groups of the Polyamide 6 materials (Fig. 2).

In order for a joining technique to be applied in an automotive setting the joint needs to withstand different aging tests in order to assure that the bond strength can be achieved throughout the lifetime of a car. Two tests among others can be used to investigate a joints aging stability. The climate change test and the salt spray test. The climate change test simulates a climate change throughout a cycle of low (−40 °C) and high temperatures combined with high humidity (+80 °C/80% relative humidity). This test enables the evaluation of two critical stresses for a hybrid fusion bond. The stress resulting from different coefficients of thermal expansion (steel and Polyamide 6) and the stress from water absorption into the fiber reinforced thermoplastic adherend. Alongside the absorption of water comes the increase of volume from water when cooled [43].

The chosen salt spray test is a hot and wet aging combined with a salt spray interval to favor possible gap-corrosion problems of a joint. This test in contrast to the climate change test only uses temperatures above room temperature and therefor the aging effects can be traced back to water absorption into the FRTP and the corrosion potential of the added salt spray solution. Both tests are difficult for hybrid fusion bonds because the aforementioned water absorption of the Polyamide 6 matrix. Due to the change of water content Polyamide 6 changes among other things the volume (see Fig. 3) and the coefficient of thermal expansion with the amount of absorbed water (see Fig. 4) as different investigations show [10,44–46].

The absorption of water in combination with low temperatures can increase the residual stresses in the material and subsequently in the joint; therefor it is necessary to understand how the joint reacts to these kinds of tests. The challenge when investigating fusion bonds is the dependability of the joint on the applied pre-treatment method and the used materials. As the investigations of [47] showed by investigating a combination of Aluminum (AlMg3) and different fiber reinforced thermoplastic materials based on a Polyamide 6.6 matrix after storing the samples in an artificial sea water environment for 21 days show. The samples cleaned with acetone failed before testing whereas the samples pre-treated with a corundum blasting (metal) and an additional polymer layer (Polyamide 6.6) achieved a lap shear strength of 9.7 MPa after aging (approximately 12 MPa before). This investigation among others shows the potential of combining a pre-treatment with hybrid fusion bonding to withstand aging tests. [47] This investigation will be focusing on aging laser pre-treated samples in order to determine if the pre-treatment in combination with a galvanized metal and a Polyamide 6 is suitable to withstand the chosen aging tests which [20] also concluded to be necessary for the future application of this joining and pre-treatment technique.

2. Materials and methods

In this section the used materials for the investigations, the applied surface pre-treatment, the sample manufacturing, the cathodic paint process and the testing methods are introduced.

2.1. Materials applied

The metal adherend for the investigations is a HX340 LAD Z100MB steel with a zinc coating. The galvanization is done in a hot-dip process according to DIN EN 10346 with a dip-coating bath of at least 99% zinc. The material properties are shown in Table 1. The other adherend is a thermoplastic glass fiber reinforced Polyamide 6 from two different

Fig. 2. Schematic interaction between a metal surface and a Polyamide 6 based on [42].

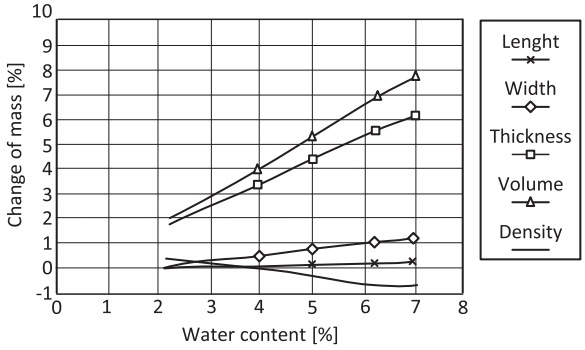

Fig. 3. Dimension changes from water absorption of a Polyamide 6 plate with 30% glass fiber content (Durethan BKV30) based on [44].

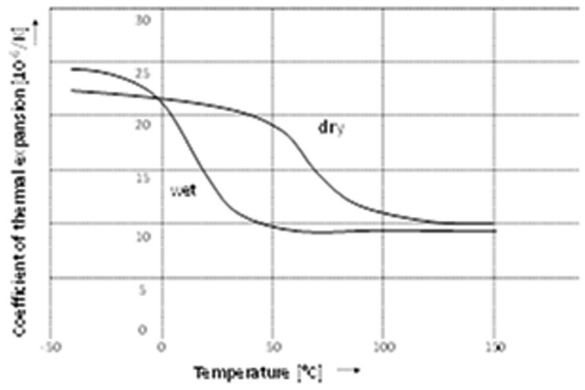

Fig. 4. Coefficient of thermal expansion for a glass fiber reinforced Polyamide 6 tissue with different water contents based on [10].

Table 1
Material properties.

Metal adherend	HX340 LAD Z100MB		
Yield strength [Mpa]	340–420		
Tensile strength [Mpa]	410–510		
Thickness t_{St} [mm]	1.5		
Coating	Zinc		
Coating grammage [g/m²]	100		
FRTP adherend	TP1a	TP1b	TP2
Matrix material	Polyamide 6	Polyamide 6	Polyamide 6
Melting temperature [°C]	≈220	≈220	≈220
Thickness t_{Pa} [mm]	2	2	2
Glass transition temperature [°C][a]	52	54	53
Fabric	Twill (50:50)	Twill (50:50)	Twill (50:50)
Fiber content [wt%][b]	64	65	63
Coefficient of thermal expansion [10^{-6}[a]1/K]	−30 – 23 °C – 19 23 – 80 °C – 15	−30 – 23 °C – 19 23 – 80 °C – 15	–

[a] Measured with Dynamic Scanning Calorimetry according to DIN EN ISO 11357-2.
[b] Measured with thermal gravimetric analysis according to DIN EN 2564.

manufacturers. Both materials have a 50:50 twill fabric fiber reinforcement with a fiber content of around 60 wt%. Under the used storage conditions (room climate with roughly 23 °C/50% r. h.) the average moisture content of the Polyamide 6 material was measured to be around 2.6 wt%. Due to a batch change the TP1 material is marked with TP1a and TP1b. The difference between the two batches could not be investigated due to the small changes which are necessary to alter the thermoplastic matrix. The difference between the two materials has become obvious after testing the reference series for the two aging tests and is therefor shown and discussed throughout this article.

2.2. Surface pre-treatment

All investigated adherends were cleaned using isopropyl before further processing. After that, the metal adherend was laser pre-treated to achieve a rougher surface structure to improve adhesion. Therefor a red Energy G4 H Type from SPI Lasers UK Limited (Southampton, United Kingdom) with an average power output of 70 W and a wavelength of 1062 ± 2 nm was used. Three different pre-treatment intensities were chosen for the pre-treatment of the cleaned surface. The settings (right) and the pre-treatment strategy (left) are shown in Fig. 5. To assure a complete pre-treatment of the joining area and to reduce edge effects the area pre-treated (16 × 27 mm) was bigger than the actual joining area (12.5 × 25 mm). The three selected laser settings represented by L1, L2 and L3 provide a low, medium and high laser pre-treatment intensity.

2.3. Manufacturing of lap-shear samples

The sample manufacturing is based on an inducer connected to a universal testing machine as it was introduced in [33]. The joining setup is shown in Fig. 7 in detail. In order to join the samples the adherends have been placed in a joining aid which provided a mechanical fusion limit at 0.1 mm (Fig. 7 on the right). After applying the joining force of 150 N with the universal testing machine which equals roughly 0.5 MPa (calculated with the joining area of 312.5 mm²) the inducer was activated and the metal sample was heated above the melting temperature of the Polyamide 6. The settings for the induction generator have been measured beforehand with thermocouples type K. For a measurement three thermocouples have been placed in the joining area (see Fig. 6). The recording was done with a sampling rate of 250 ms with a 34970 A Data Logger Switch Unit from Keysight Technologies Inc. (Santa Rosa, USA). After acquiring the settings for the induction generator the temperature was measured again with the same setup and five different samples. The final temperature during the joining process was 240 ± 10 °C. The average temperature of the three thermocouples and the five measurements is shown in Fig. 6. The envelope (dashed red lines) resembles the standard variation of the five measurements. After defining this heating strategy, samples were built without further temperature control in order to achieve a joining area without thermocouples.

The dwelling time was set to be seven seconds with a two second heating rate. After the dwelling time the pressure was kept constant for the sample cooling. This was done with pressurized air for ten seconds. Finally the samples were taken out of the joining aid and ready for the cathodic paint.

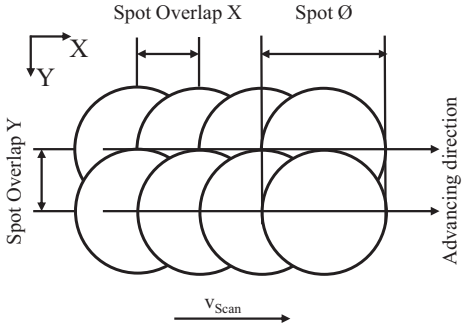

	f [kHz]	P_{Avg} [W]	SO_X [%]	SO_Y [%]
L1	60	70	72	50
L2	60	70	72	95
L3	60	70	83	95

Fig. 5. Laser pre-treatment strategy (left) and laser settings (right) [10].

2.4. Preparation of micro sections of joined lap-shear samples

For analyzing the wetting of the metal surface and additional information about the surface structures provided by the laser pre-treatment micro sections of joined samples have been made. Therefor the joined sample was cut several times with a wet cut-off machine in order to have a sample small enough for the embedding procedure (Fig. 8). Due to the temperature sensitivity of the joint a cold embedding process was used (scandiquick from SCAN-DIA GmbH (Hagen, Germany)). After embedding the samples have been grinded and polished before the images were acquired with a Leica DM 4000 M microscope from Leica Microsystems GmbH (Wetzlar, Germany).

2.5. Surface analysis

The non-destructive surface characterization is done by using a scanning electron microscope and a stylus instrument. All applied methods will be explained in the following paragraphs.

The scanning electron microscopy (SEM) recordings have been acquired with a FEM Quanta FEG 650 from Thermo Fisher Scientific Inc. (Waltham, USA). The secondary electron detector was an Everhart-Thornley-Detector from Thermo Fischer Scientific Inc. (Waltham, USA). The sample size for the SEM investigations was 25 mm × 15 mm. The HX340 steel was cleaned with isopropyl before applying the laser pre-treatment. Furthermore the samples have been carefully blasted with Nitrogen before evacuating the SEM in order to remove loose residues (spatters) from the surface that would otherwise interfere with the electron beam.

In addition, an energy dispersive X-ray (EDX) analysis of the resulting surfaces was conducted. The sensor used for these measurements was a X-Max^N detector with a detection area of 80 mm^2 from Oxford Instruments plc (Abingdon, United Kingdom) and a resolution of 127 eV at 5.9 keV. Due to the small surface area that can be scanned with the EDX (roughly 0.11 mm^2) at least three areas per sample on three different samples have been investigated in order to achieve statistic relevance. The measurements of one pre-treatment setting as well as the cleaned surface are an average of nine measurements on three different samples. The acceleration voltage during all EDX measurements was kept constant at 10 kV.

The surface roughness measurements have been done with a MarSurf M400 stylus instrument from Mahr GmbH (Goettingen, Germany). The measuring distance for acquiring the average surface roughness (R_a) was set to 5.6 mm. The measuring direction was crosswise to the laser pre-treatment direction. To achieve a statistic relevance three lines per sample on three different samples have been measured.

2.6. Aging of samples

In order to prevent a corrosion of the cutting edges of the metal adherend all samples have been coated in a cathodic paint process after the joining process. If these cutting edges are not properly coated before the aging test, the samples would only show an infiltration-corrosion between the zinc coating and the steel substrate. The cathodic paint coating was chosen because it enables a coating which is limited to the metal adherend due to the necessity of a conductive material. This way only the metal adherend is coated without a coating of the thermoplastic glass fiber reinforced material. The cathodic paint used for coating is an epoxy based system used in the automotive industry. After the application of the cathodic paint, the samples have been cured in an oven at 180 °C for 30 min. In cases were a cathodic paint wasn't necessary, e.g. reference samples, the samples have also been exposed to a drying process by placing them in a laboratory oven for 30 min at 180 °C. In order to compensate the drying of the thermoplastic material from the cathodic paint process the samples rested for at least one week at 23 °C and 50 °% r. h. before testing. After the cathodic paint the samples were aged with a climate change and a salt spray test.

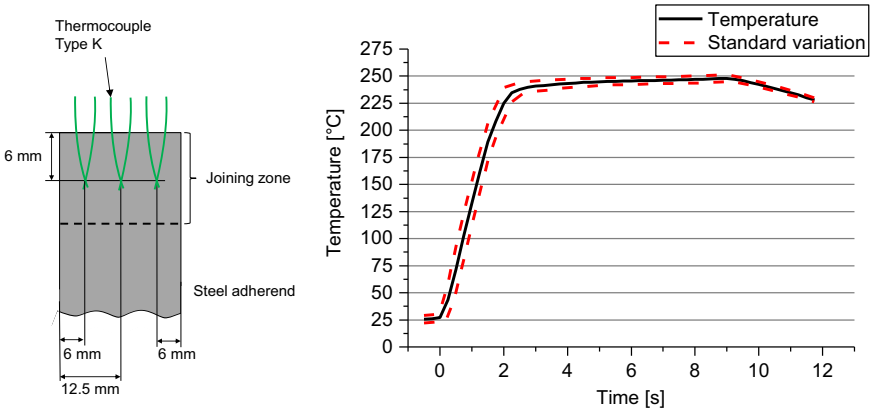

Fig. 6. Temperature measurements for the chosen heating settings.

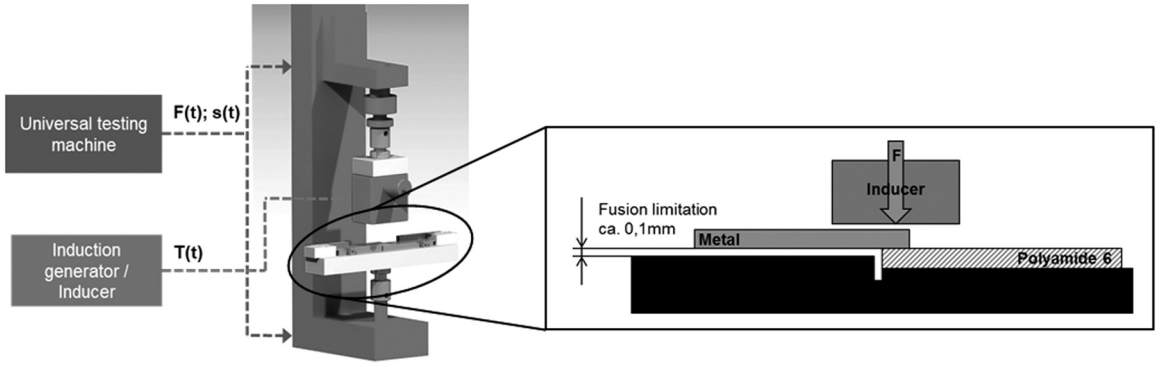

Fig. 7. Assembly setup (left) and joining aid with melt limitation for both setups (right) [33].

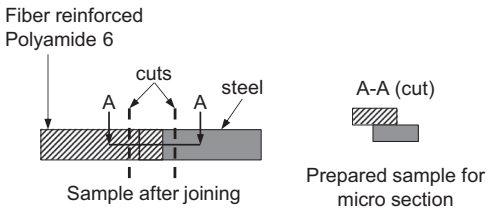

Fig. 8. Preparation of samples for micro sections.

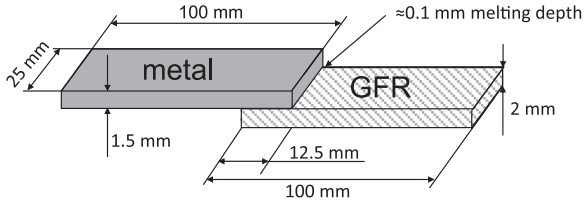

Fig. 9. Sample geometry based on DIN EN 1465.

2.6.1. Aging of samples under climate change conditions

The aging of samples under climate change conditions was done by using a test from the Volkswagen Group specified as PV1200. The test consists of two dwelling times of four hours at −40 °C and +80 °C/80% relative humidity. The dwelling times are connected with a heating resp. cooling phase of two hours to switch between low and high temperatures during a cycle. To be able to investigate the impact of the climate change on the resulting lap-shear strength, samples have been tested after 30, 60 and 100 cycles. The additional steps have been added to understand the behavior of the fusion bonds throughout the test. To achieve a comparable state between the different cycle times, the samples have been stored at room climate (23 °C and 50 °% r. h.) for a week before testing.

2.6.2. Aging of samples with salt spray test

The salt spray test applied to the samples was also a test of the Volkswagen Group specified as PV1210. This test is based on a salt spray test of four hours according to DIN EN ISO 9227, followed by a dwelling time of four hours at 23 °C/50% rel. humidity and a 16 h dwelling time at a warm-wet-climate of 40 °C/100% rel. humidity according to DIN EN ISO 6270-2. To be able to investigate the influence of the salt spray test on the resulting lap-shear strength samples have been tested after 30, 60 and 90 cycles. Again the additional steps of 30 and 60 cycles have been added to better understand the aging behavior of the samples. In order to have comparable results the samples have been conditioned at room climate for a week before testing like it was done during the test of climate change conditions.

2.7. Single lap-shear test

The lap-shear strength (joint strength) in this investigation is determined by using the single lap-shear test according to DIN EN 1465. The fusion bond is built from a Polyamide 6 adherend with glass fiber reinforcement (GFR) and a steel adherend as shown in Fig. 9. The testing speed is set at 10 mm/min. The tests have been carried out on a universal testing machine (model 5966) from Instron (Illinois Tool Works Inc., Glenview, USA).

After testing, the resulting fracture patterns have been documented and categorized based on DIN EN ISO 10365. The characterization of the fracture patterns is shown in Table 2.

3. Results

In the first part of this section the results of the laser pre-treatment will be discussed therefor SEM recordings are presented and to give a measureable scale for the surface structures roughness measurements are added. Finally the surface elements detected with the EDX for different surface states are shown. After the surface analysis, the results of the lap-shear tests are shown in detail.

3.1. Analysis of the surfaces

In this section the results of the scanning electron microscopy and additionally performed surface roughness measurements are introduced before the results of the surface chemistry investigations are shown.

3.1.1. Scanning electron microscopy

The surface before a laser pre-treatment has been applied is shown in Fig. 10 on the left side. The surface shows a typical structure for a zinc coated metal surface. The structure of the surface does not provide visible undercuts. In comparison the surface pre-treated with the low pre-treatment intensity of parameter setting L1 shows a change of the surface topology. The surface shows a reoccurring structure which potentially provides a better mechanical interlocking than the initial state of the HX340.

By reducing the spot overlap in Y-direction the parameter setting L2 achieves a higher pre-treatment intensity than the previously discussed L1. The surface topology changes again as can be seen in Fig. 11 (left) into a more even distributed structure with a wavelike structure underlying the smaller structures. Furthermore, the structures are now coated with a fuzzy structure as the image on the right shows (Fig. 10). The laser structuring tends to provide a surface modification on different scales which should improve the adhesion of thermoplastic material.

Another increase of the pre-treatment intensity by additionally reducing the spot overlap in X-direction changes the resulting surface topography again. The surface created with L3 shown in Fig. 12 is characterized by a multitude of undercuts and a rough looking surface. Again the surface topography is changed on different scales as the

Table 2
Characterization of fracture patterns from hybrid fusion bonds based on DIN EN ISO 10365.

Adhesion Failure	Cohesion Failure	Delamination Failure	Cohesive substrate Failure
AF	CF	DF	CSF
		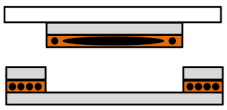	
No residues of thermoplastic matrix on metal adherend	Residues of thermoplastic matrix on metal adherend	Visible fiber residues on metal adherend	Substrate failure from corrosion
			
metal adherend	fiber reinforced thermoplastic adherend: thermplastic matrix + fiber layer		

magnified image on the right shows. Again a fuzzy structure covering the base material can be observed.

In order to achieve a better understanding of the structure of this fuzzy covering a smaller scale image was made. This image is shown in Fig. 13. The image with a scale of 500 nm shows that the fuzzy structure seems to grow from the base material. Furthermore the structure should get infiltrated by the thermoplastic material due to the open structure.

3.1.2. Surface roughness measurements

In order to provide a measurable value to these surface topography changes through a laser pre-treatment the surface roughness was measured with a stylus instrument. The initial state of the HX340 surface was measured with a R_a of 1.09 ± 0.05 µm. When the surface is laser pre-treated the surface roughness was slightly increased for the lowest pre-treatment intensity as the R_a of 2.15 ± 0.17 µm shows. A further increase of pre-treatment intensity by applying L2 to the HX340 surface results in an average surface roughness of 2.22 ± 0.53 µm. L2 does not provides a significantly higher surface roughness but as the SEM recordings show the surface topography changes significantly with the different pre-treatment settings. The highest investigated pre-treatment intensity of L3 reaches an average surface roughness of 6.16 ± 0.45 µm.

3.1.3. Investigation of the surface chemistry

After providing SEM images and surface roughness measurements the surface was also investigated with an energy dispersive X-Ray spectroscopy in order to measure the present surface elements before and after a laser pre-treatment. The results of these measurements are shown in Fig. 14 for the initial (cleaned) state of the HX340 material and the three different laser settings (L1, L2 and L3).

The cleaned surface shows a zinc share of nearly 92.3 ± 0.6% the aluminum (1.4 ± 0.3%) seems to be a part of the zinc coating composition whereas the oxygen and carbon amounts could stand for a certain degree of surface contamination that is still present after the cleaning with isopropyl. Compared to the standardized process of the galvanization procedure the amount of aluminum seems to be too high when a galvanization with at least 99% zinc should be used. The small but measurable amount of iron with 0.8 ± 0.2% should be an element

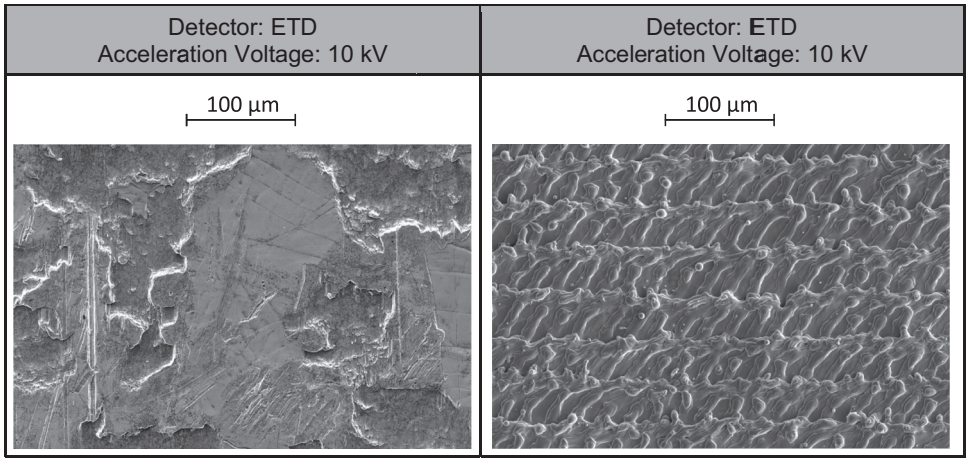

Fig. 10. SEM images of the untreated HX340 surface (left) and the laser pre-treated HX340 surface with low intensity L1 (right).

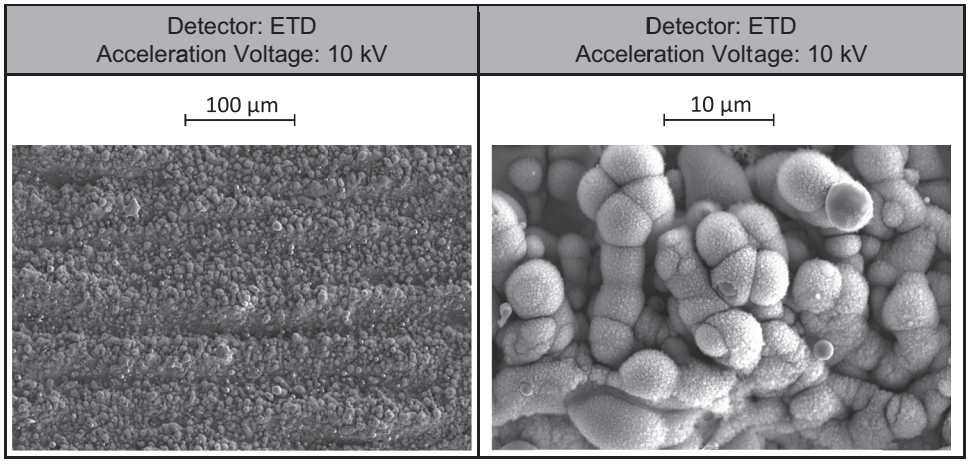

Fig. 11. SEM images of the laper pre-treated HX340 surface with medium intensity L2 in different scales.

provided by the base material which is present due to the depth effect of a X-ray measurement.

When a laser pre-treatment is applied the composition of the surface elements changes significantly. The lowest pre-treatment intensity of L1 results in a reduction of zinc concentration on the surface to 16.0 ± 5.8% whereas the iron portion increases up to 74.0 ± 5.7%. Along with the increase of iron the amount of oxygen increases from 1.9 ± 0.3% (cleaned) to 6.9 ± 0.6%. The aluminum content measured on the cleaned surface is not detected after a laser pre-treatment with a low intensity. An increase of the pre-treatment intensity with laser setting L2 results in the lowest concentration of zinc on the surface with only 10.3 ± 1.6%. In comparison to L1 the decrease of zinc does not correlate with an equally high amount of iron on the surface (67.7 ± 2.5%). In comparison the amount of oxygen increases significantly to 19.4 ± 1.8% which could hint at a oxidation of the metal adherend. Aluminum has not been detected on the surfaces after a pre-treatment with a medium intensity as it was the case for low intensities.

This effect increases when the highest pre-treatment intensity of L3 is applied to the surface. The amount of zinc is the highest of all investigated pre-treatment intensities (23.7 ± 6.3%) and the concentration of iron is the lowest with only 52.4 ± 6.8% with no aluminum present after the pre-treatment. Again the oxygen amount is high with 21.0 ± 0.7%. The changes of L2 and L3 especially of zinc and iron are close together when the standard deviation is taken into account. The most significant difference between L1 and L2/L3 is the amount of oxygen.

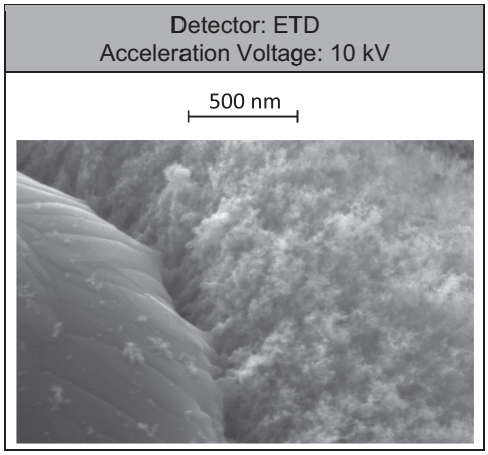

Fig. 13. SEM image of the laser pre-treated HX340 surface with the highest intensity L3 and a 500 nm scale.

3.2. Investigation of hybrid fusion bonds

In this section the results of micro sections of joined samples and two different aging tests are shown. The investigation begins with the micro sections before the samples tested under climate changing conditions and the results of the salt spray test are shown. All results are accompanied by selected fracture patterns.

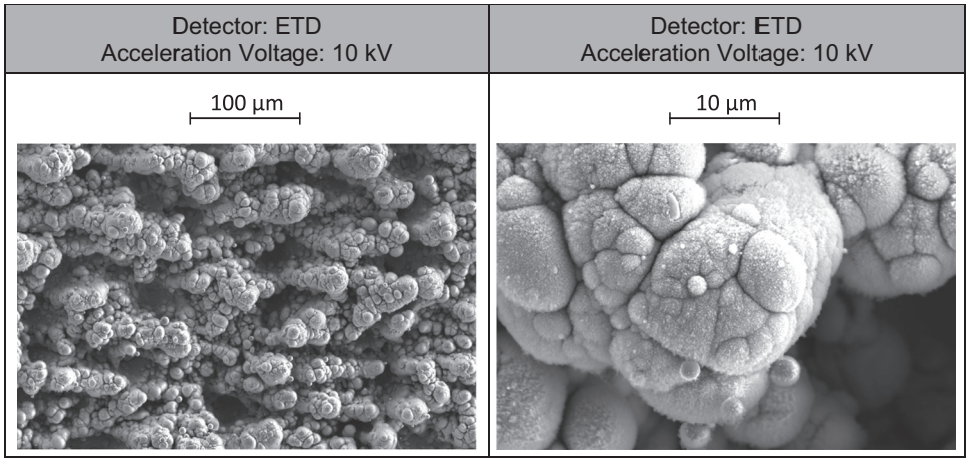

Fig. 12. SEM images of the laser pre-treated HX340 surface with highest intensity L3 in different scales.

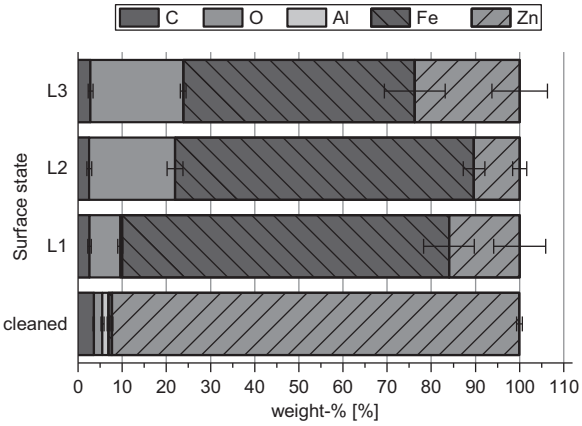

Fig. 14. EDX-measurements of HX340 surfaces before and after laser pre-treatment with different laser pre-treatment intensities.

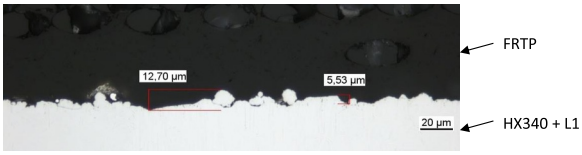

Fig. 15. Micro section of a joined sample pre-treated with L1 (lowest intensity).

3.2.1. Investigation of micro sections

The micro section of a surface pre-treated with a low intensity (L1) is shown in Fig. 15. The reoccurring pattern which is visible in the SEM images (see Fig. 10) is characterized by small melting ejections. The molten material forms small undercuts on the surface which depending on the cut are more or less connected to the base material. An increase of the pre-treatment intensity with laser setting L2 is shown in Fig. 16.

The increased pre-treatment intensity leads to smaller structures with a more wavelike structure as it was already observed in the SEM recordings (see Fig. 11). The slight decrease of the surface heights observed in these micro section compared to the low intensity does not show in the surface roughness measurements (see Section 3.2.1). The pre-treatment of the HX340 material with a high pre-treatment intensity is shown in Fig. 17.

A further increase of pre-treatment intensity results in a surface which shows significantly higher structures and also better possibilities for mechanical interlocking of the thermoplastic material into the surface.

All micro sections show a good bonding of the thermoplastic material to the investigated surfaces which is the result of the temperature input from the steel material into the thermoplastic material. This helps to prevent a shock curing of the thermoplastic material and a drop of viscosity in the boundary layer by constantly heating the metal adherend throughout the joining process. Furthermore the constant pressure during the cooling of the samples results in no visible pores.

3.2.2. Investigation of hybrid fusion bonds under climate change

The investigations of lap-shear samples before and after different cycles of a climate change test are shown in Fig. 18. The results show a

Fig. 16. Micro section of a joined sample pre-treated with L2 (medium intensity).

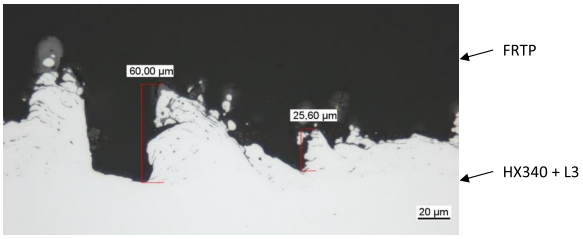

Fig. 17. Micro section of a joined sample pre-treated with L3 (highest intensity).

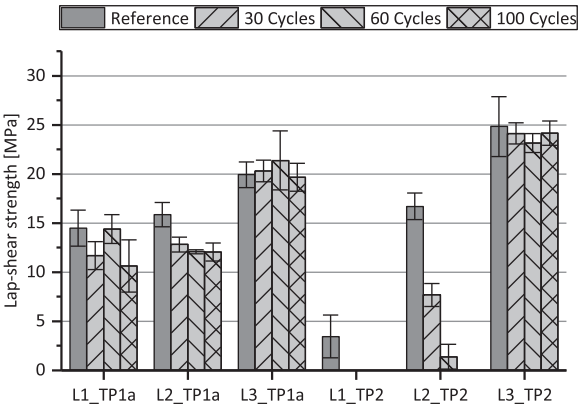

Fig. 18. Results of aged samples after climate change.

different behavior for the two investigated materials as well as for the selected laser pre-treatment settings. The examination of the climate test will start with the TP1a material before the TP2 material is looked at.

The TP1a material achieves a lap-shear strength of 14.5 ± 1.8 MPa after the cathodic paint oven which is the reference for this test. After aging the samples for 30 cycles, the lap-shear strength decreases to 11.7 ± 1.4 MPa. The results after 60 cycles show an inconsistent behavior because the resulting lap-shear strength is recorded with 14.4 ± 1.5 MPa. After 100 cycles the lap-shear strength drops again to 10.6 ± 2.6 MPa. The results of the aged samples of TP1a with L1 have nearly no overlapping standard variation and therefor the results after 60 cycles cannot be explained. The results of this test series show a consistent behavior for 30 and 100 cycles especially when they are compared with the results of TP1a with a medium pre-treatment intensity (L2). The results of TP1a with L2 show a decrease of achievable joint strength from the initial value (15.9 ± 1.2 MPa) of −20% to 12.8 ± 0.8 MPa (30 cycles). The further aging of the samples (60 and 100 cycles) does not change the lap-shear strength. This result was also expected for the samples joined with L1. An increase of the pre-treatment intensity to laser setting L3 increases the strength of the reference to 19.9 ± 1.3 MPa. Contrary to the aforementioned settings (L1 and L2) this pre-treatment does not result in a decrease of lap-shear strength due to the aging process (30 cycles: 20.3 ± 1.1 MPa; 60 cycles: 21.4 ± 3.0 MPa; 90 cycles: 19.7 ± 1.4 MPa). All tested samples achieve the same joint strength as the reference samples when the standard variation is concerned.

The aging of the TP2 material shows different results for the climate change aging. A pre-treatment with laser settings L1 results in a lap-shear strength of 3.4 ± 2.2 MPa for the reference samples. This low joint strength results in a complete failure of the joint already after 30 cycles. An increase of the pre-treatment intensity with laser setting L2 results in a higher lap-shear strength for the reference samples of 16.7 ± 1.4 MPa. But after aging the samples for 30 cycles the strength decreases by more than half to only 7.7 ± 1.1 MPa. This decreasing trend continuous for the samples after 60 cycles (1.4 ± 1.3 MPa) until a

Table 3
Selected fracture patterns of specimens after climate change.

	Reference	30 Cycles	60 Cycles	100 Cycles
TP1a L1				
Fracture pattern	CF/DF	CF	CF	CF
TP1a L3				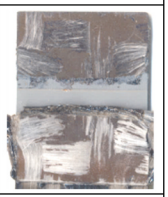
Fracture pattern	DF	DF	DF	CF/DF
TP2 L1				
Fracture pattern	AF	AF/CSF	AF/CSF	AF/CSF
TP2 L3				
Fracture pattern	CF/DF	CF	CF/DF	CF/DF

complete failure after 100 cycles was observed. The highest investigated pre-treatment intensity (L3) achieves a lap-shear strength after the cathodic paint of 24.8 ± 3.0 MPa. After aging the samples for 100 cycles the joint strength is still on the same level as before (24.2 ± 1.2 MPa). To close the investigations about the aging under climate changing conditions Table 3 shows selected fracture patterns of the lap-shear tests.

The fracture patterns for the TP1a material show only minor differences for the samples pre-treated with L1 although the results of the lap-shear strength show an inconclusive behavior. The fracture patterns cannot explain the increase of lap-shear strength after 60 cycles which result in the same cohesive fracture pattern as the samples tested after 30 and 100 cycles. The decrease of the lap-shear strength after 30 and 100 cycles could be explained by the missing fiber residues on the metal adherend after testing but this can also be observed at the samples after 60 cycles which resulted in the same strength as the reference. Therefor the results of this pre-treatment setting (L1) are still inconclusive. A pre-treatment with the highest pre-treatment intensity (L3) results in a complete failure of the first fiber layer (DF). This fracture pattern can also be observed after 30 and 60 cycles only after 100 cycles the amount of delamination failure seems to be reduced but without any effect on the achievable lap-shear strength as the results show.

The TP2 material in comparison shows for all investigated pre-treatment intensities fewer fiber residues on the metal adherend after testing. The samples pre-treated with L1 show an adhesion failure (AF) after the cathodic paint. Due to the climate change aging the samples failed after 30 cycles the fracture patterns show first signs of corrosion which resulted in the failure of the joint. This corrosion increases with the ongoing aging. In contrast the samples pre-treated with the highest pre-treatment intensity show minor fiber residues after the cathodic paint. These cannot be observed after 30 cycles but reoccur after 60 and 100 cycles. The differences in the fracture patterns did not result in a difference in lap-shear strength which could be a hint that the fibers did not fracture but are pulled out due to their orientation at the cutting edges. After discussing the fracture patterns of the climate changing tests the results of the salt spray test will be introduced.

3.2.3. *Investigation of hybrid fusion bonds after salt spray test*

The investigations of lap-shear samples before and after different cycles of a salt spray test are shown in Fig. 19.

The results show a dependency between the chosen material as well

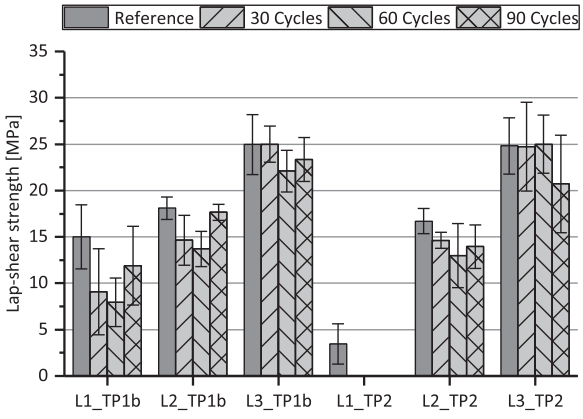

Fig. 19. Results of aged samples after salt spray test.

as the selected laser pre-treatment settings and the resulting lap-shear strength. The TP1b material joined with a low pre-treatment intensity shows a loss of lap-shear strength to 9.1 ± 4.6 MPa compared with the reference (15.0 ± 3.5 MPa) after only 30 cycles. The further aging does not change the performance of the joint when the standard variation is taken into account. The increasing of laser pre-treatment intensity with L2 achieves a more stable result when the standard variation of the aged samples is taken into account but a marginal loss of performance can be observed. Compared to the reference of 18.1 ± 1.2 MPa the lap-shear strength after 30 cycles decreased to 14.6 ± 2.7 MPa. After 90 cycles the lap-shear strength increases slightly to the strength of the reference samples. But due to the standard variation of the different cycle times the results show only a minor trend for a decrease of lap-shear strength due to the salt spray testing. The results in combination with the highest pre-treatment intensity (L3) in combination with TP1b show the highest lap-shear strength with TP1b (Reference: 25.0 ± 3.2 MPa) and realize a nearly constant behavior over the investigated length of the salt spray test (90 cycles: 23.3 ± 2.4 MPa) especially when the standard variation is concerned.

The results of the TP2 material show a different behavior after the salt spray tests. The samples pre-treated with the lowest intensity showed already a lower lap-shear strength of 3.4 ± 2.2 MPa compared to TP1b when the reference was tested. The results after salt spray test resulted in a total failure of the joint. This changes when the pre-treatment intensity is increased with parameter setting L2. The reference achieves a lap-shear strength of 16.7 ± 1.4 MPa. The testing after 30 cycles results in a lap-shear strength of 14.6 ± 0.9 MPa which does not change over the following periods as the result after 90 cycles with 14.0 ± 2.3 MPa shows. As with TP1b the highest lap-shear strength is achieved by applying the highest pre-treatment intensity L3 to the metal surface. The reference achieves a lap-shear strength of 24.8 ± 3.0 MPa. The samples after 30 and 60 cycles achieve comparable lap-shear strength when the standard variation is concerned. The only decrease of lap-shear strength can be seen after 90 cycles with an average lap-shear strength of 20.7 MPa but the standard variation is high (± 5.2 MPa) compared to the other cycles. This high standard variation is due to one sample which showed corrosion signs. Without this spike the average lap-shear strength is 22.3 ± 3.9 MPa. To better understand the results of the aging tests Table 4 shows selected fracture patterns.

The selected fracture patterns of the salt spray test show in case TP1b the samples pre-treated with a low pre-treatment intensity (L1). The reference samples show a complete cohesive failure with fiber residues on the surface (delamination failure of the thermoplastic part). The fracture pattern shows also that the fibers have become visible which indicates that the failure has occurred between fiber and matrix and not between surface and matrix material. When the samples are exposed to a salt spray aging the fracture pattern after 30 cycles already shows first signs of corrosion (cohesion substrate failure of the metal substrate) especially at the long edges of the lap-shear specimen. This first corrosion signs are an explanation for the reduction of lap-shear strength and the increase of standard variation because the severity of the corrosion differs from sample to sample. As the difference in achievable lap-shear strength with TP1b and L1 does not show a trend over the time of aging the resulting fracture patterns also do not show significant differences. The fracture patterns of TP1b pre-treated with the highest intensity (L3) show a cohesive failure of the thermoplastic matrix for the reference samples without fiber residues on the metal adherend. This fracture pattern does not change throughout the aging of the samples which correlates with the constant lap-shear strength recorded after the samples aging.

The fracture patterns of TP2 and L1 show the difference for the two investigated materials after aging. The samples show an adhesion failure in the reference test but a complete joint failure after 30 cycles with a severe and visible corrosion (CSF) in the joining area. This corrosion leads to a failure of the samples before testing even though cohesion was achieved as residues of thermoplastic material on the metal adherend show. The further aging of the TP2_L1 samples only leads to an increase of corroded area until the fracture pattern of 90 cycles shows a complete corrosion of the bonding area. In contrast the medium and high pre-treatment intensities of L2 and L3 achieve a cohesive failure throughout the aging test. Due to the small differences only L3 is shown in Table 4. The reference sample shows a cohesive failure which as stated before does not change for 30 and 60 cycles which correlates with the recorded lap-shear strength of the samples. The fracture pattern after 90 cycles only shows minor differences with one spike that showed signs of corrosion which is suitable to explain the high standard variation of this sample series.

4. Discussion

In this chapter the aforementioned results will be discussed in detail. The discussion starts with the comparison of the surface analysis and the impact of a batch change of the FRTP before the focus is put on the results of the two carried out aging tests.

4.1. Discussion of surface analysis

The surface analysis shows that the pre-treatment with a laser has an impact on the surface topography as well as the surface chemistry. The effect on the surface is caused by the interaction between the laser beam and the surface. Due to the zinc coating the laser pre-treatment encounters a surface with a lower melting point than the base material. For zinc the melting temperature is roughly 419 °C and the boiling temperature is around 907 °C both temperatures are under the melting temperature of iron (1537 °C) [48]. The energy provided during the laser pre-treatment for melting the steel as it was observed in the SEM images and micro sections should be high enough to at melt resp. sublimate the zinc coating which is the explanation for the reduction of zinc on the pre-treated surfaces. The high temperatures during the pre-treatment could also result in iron, zinc and oxygen compounds like franklinite (Fe_2ZnO_4) [49] or other compounds which are known from other high temperature surface pre-treatments utilized on galvanized surfaces e. g. galvannealing processes. During this process an iron-zinc compound (e. g. $FeZn_{10}$) is formed [50]. A laser pre-treatment of a metal surface causes a significant change of the interface chemistry which influences the aging behavior. As the investigation from [42] showed higher amounts of oxides on the metal surface should increase the possibility for the formation of hydrogen bonds with the amide groups of the Polyamide 6. The low and medium pre-treatment intensity achieve nearly the same surface roughness but the surface chemistry between these two settings is different. Whereas the surface roughness of a medium and high pre-treatment intensity is different but the surface chemistry is similar, considering the standard variation of the investigations. This enables the evaluation of the predominant joining mechanism (mechanical interlocking or specific adhesion). Especially the results of the surface elements measured with the EDX need to be interpreted carefully. To achieve this several surface areas per sample (three) and several pre-treated samples (at least three) have been measured. But especially on the rough surfaces of laser setting L3 shadowing effects occurred, due to the measuring technique of the EDX detector which measures under an angle of roughly 30°. To compensate this shadowing effect the final measuring areas have been chosen by the signal strength so shadowed areas have not been considered for evaluating the surface elements. Furthermore the detection with an EDX also incorporates not only information from the surface elements but due to the penetration of the x-rays into the sample also information from the base material. This penetration effect of the EDX measurement can be accepted in this investigation because the samples are only compared with each other and therefor a change in composition can be traced back to a change of the surface composition due to the laser pre-treatment.

Table 4
Selected fracture patterns of specimens aged with salt spray test.

	Reference	30 Cycles	60 Cycles	90 Cycles
TP1b L1				
Fracture pattern	CF/DF	CF/CSF	CF/CSF	CF/CSF
TP1b L3				
Fracture pattern	CF	CF	CF	CF
TP2 L1				
Fracture pattern	AF	AF/CSF	AF/CSF	CSF
TP2 L3				
Fracture pattern	CF	CF	CF	CF

4.2. Discussion of TP1 batch change

The results of the two reference series reveals that a batch change of the TP1 material can have significant effects on the achievable lap-shear strength of the hybrid joint. The difference between TP1a (14.5 ± 1.8 MPa) and TP1b (15.0 ± 3.5 MPa) can be neglected for the lowest pre-treatment intensity. However, an increase of pre-treatment intensity to L2 shows an improvement of the achievable lap-shear strength for the newer batch (TP1b). TP1a reaches 15.9 ± 1.2 MPa whereas TP1b achieves slightly higher lap-shear strength (18.1 ± 1.2 MPa). But the differences are still minor considering the lap-shear results and the differences in fracture patterns. The results change for the highest investigated pre-treatment intensity were the TP1a material achieves a lap-shear strength of 19.9 ± 1.3 MPa with a complete failure of the first fiber layer (see Table 3). In contrast, the TP1b material achieves 25.0 ± 3.2 MPa without a failure of the first fiber layer (see Table 4).

Unfortunately, the changes of the manufacturing process of the semi-finished products (TP1a to TP1b) could not be revealed by the authors and therefor only possible changes can be addressed. Due to the change of the fracture pattern from a delamination failure to a cohesive failure two possible changes could have been made by the manufacturer of the fiber reinforced thermoplastic material. The composition of the thermoplastic material could have been changed or the facing of the glass fiber was changed without a change of the thermoplastic matrix. By changing the facing the adhesion between the thermoplastic and the fibers could be improved. This could lead to a better load introduction into the deeper fiber layers which results in a failure of the thermoplastic material without fiber failure, theoretically resulting in the present fracture pattern. When the composition of the matrix material is altered the material could provide better adhesion to the fibers and the metal adherend which could also lead to a change of the resulting fracture pattern. The changes made had a severe impact on the achievable lap-shear strength as the results of the two different batches showed. On the hand the differences for the low and medium pre-treatment intensities do not change as significantly which makes the change of the facing more plausible than an improved adhesion of the matrix due to a change of composition. The composition of Polyamide 6 materials is very complex and therefor not revealed by the manufacturer but this investigation shows the severe impact a batch change can have on the outcome of a test. This problem was intentionally addressed in this investigation because it shows that a change to the composition can be crucial for a later implementation.

4.3. Discussion of the results after the climate changing test

The climate changing test shows that the performance is influenced by the FRTP as well as the chosen pre-treatment settings. The TP1a material shows nearly the same behavior on all investigated metal surfaces. Low and medium pre-treated surfaces show a minor loss of lap-shear strength whereas surfaces with high pre-treatment intensities show no impact due to the climate changing test. In comparison the TP2 material shows to be impacted by the climate changing conditions quite severe. The material fails on surfaces pre-treated with L1 after 30 cycles and on L2 the performance drops until complete failure after 100 cycles. Due to the good performance of TP2 on surfaces pre-treated with

the highest investigated intensity (L3) it seems that the material needs a rougher surface in order to achieve stable aging results under climate changing conditions. The same can be stated for the TP1a material.

The fracture during the climate changing test could occur due to two different effects. One is the change of temperatures and along with that the mismatch of the thermal expansion of the two adherends. Unfortunately, only the TP1 material was supplied with a data sheet that included information on the coefficient of thermal expansion (CTE) in detail but it can be assumed that the CTE of the TP2 material is close to the one of TP1a due to the same fiber layout. However, the CTE mismatch between a glass fiber reinforced material and steel is small 15–19 * 10^{-6}/K compared to 12 * 10^{-6}/K (for steel according to [48]) which indicates ~~to~~ another failure mechanism. The other possibility is due to the absorption of water from the thermoplastic matrix as shown by [44] and the subsequent change of volume (by absorbing water and of water itself when cooled) of the Polyamide 6. Both effects create stresses in the joint which can lead to a decrease of the lap-shear strength throughout the aging cycles. The decrease of TP2 pre-treated with L2 could show a slight decrease from the ongoing changes of water content and temperature. The rougher surfaces provide a better topography with more and deeper undercuts to handle stresses from the volume changes and the differences of the thermal expansion of the investigated materials as the results with both materials show. These surfaces and the resulting interlocking of the matrix in the undercuts means that the matrix cannot slip out, as easy as it is the case for surfaces pre-treated with L1 and L2. In an earlier investigation concerning the joint strength under different testing temperatures the TP2 material in combination with L1 showed a drop of lap shear strength when tested at −40 °C whereas L3 showed increased lap-shear strength. Therefor, the combination of low temperatures and surfaces pre-treated with L1 seem to be a challenge for the TP2 material [33]. The low temperatures in combination with a low surface roughness lead to the conclusion that the material is relying more on interlocking than on adhesion to the surface.

4.4. Discussion of the results after the salt spray test

The joints with a steel adherend pre-treated with the lowest intensity are very unstable for the TP1b material as the high standard variation shows. In combination with TP2, the joint fails before testing after 30 cycles. The other pre-treatment settings achieve better results, which could be explained with the different surface chemistry of the metal adherends after the laser pre-treatment.

The L1 setting achieves the lowest amounts of oxygen and the highest amounts of iron on the surfaces. This surface in comparison to the higher pre-treatment intensities which achieve high oxygen and low iron concentrations on the surface seems to be more accessible to corrosion. The already oxidized surfaces (highest amounts of oxygen) of the medium and high pre-treatment intensities do not show corrosion signs comparable to the ones seen on surfaces pre-treated with low intensities. Due to the more accessible surface of L1 a gap corrosion process is started which is supported by the corrosive agent and the high temperatures during the test. The progression of this gap corrosion can be retraced by the resulting fracture patterns of TP2 and L1 over the different aging cycles. After 30 cycles the corrosion can be seen especially at the samples edges (see Table 4). With further aging the corrosion reaches the inner parts of the joining area (60 cycles) before the whole joining area is corroded (90 cycles). Consequently, the joint cannot provide a sufficient strength throughout the aging test. Even if not as severe as for TP2 the TP1b material shows a similar behavior especially when longer aging cycles are concerned. Furthermore, the results of the salt-spray test show that the absorption of water itself without low temperatures does not seem to influence the joint strength as the direct comparison with the results of the climate change of TP2 with L2 shows.

Overall the investigations show that the samples can be passivated with a cathodic paint process in order to prevent infiltration corrosion from the cutting edges of the lap-shear sample. As the investigation of the TP2 material in combination with L1 shows a limitation of the impact of the chosen corrosion test cannot be concluded due to the severe corrosion that has been observed for this pre-treatment setting. The results show that the aging performance under salt spray conditions can also be influenced by the selection of the laser pre-treatment setting as the results of TP2 on L1 resp. L2 and L3 show. A comparison between the climate change test and the salt spray test of the TP1 material is only done for the reference samples (see Section 4.2) due to the batch change a comparison cannot be done for the aged samples.

5. Conclusion

The climate changing test seems to be the tougher test for the investigated fusion bonds which could be explained by the combination of the CTE mismatch of the adherend materials, the combination of absorbed water and the volume increase of water due to low temperatures. In comparison to the hot and wet cycles of the salt spray test the water absorption itself, without low temperatures, does not seem to be as critical especially when looked at TP2 in combination with L2. Furthermore surfaces with higher zinc residues and more oxygen show better (more stable) results throughout the salt-spray test for both materials. The laser pre-treatment therefor should focus on achieving a suchlike surface chemistry. Overall the investigations show that both tests can be fulfilled with fusion bonds if the a pre-treatment setting is used that achieves a surface roughness around an R_A of 6.16 ± 0.45 µm (for this investigation) and a surface that is dominated by oxides.

For future investigations a combined test with climate change and salt-spray test should be carried out. Additionally the volume changes of the FRTP from water absorption with and without low temperatures should be investigated in order to be able to correlate the shape changing of the material and the aging stability. Additionally an investigation of the FRTP composition should be carried out in order to better understand the effects of different batches on the resulting joint performance as it was shown in this investigation. Furthermore a better understanding of the surface chemistry of the laser pre-treated steel adherend in order to provide a better explanation for the chemical interrelations between the pre-treated surfaces and the corrosive agent is necessary. In order to achieve a better understanding of the created oxide layer environmental scanning electron microscopy of the already built micro sections will be done in order to provide information about thickness of the generated oxide layer and a possible infiltration with Polyamide 6.

Acknowledgements

This research and development project is funded by the German Federal Ministry of Education and Research (BMBF) within the Forschungscampus “Open Hybrid LabFactory” (02PQ5100) and managed by the Project Management Agency Karlsruhe (PTKA). The authors are responsible for the content of this publication.

References

[1] Fleischer J, Teti R, Lanza G, Mativenga P, Moehring H-C, Caggiano A. Composite materials parts manufacturing. CIRP Ann 2018;67(2). https://doi.org/10.1016/j.cirp.2018.05.005.

[2] Heuss R, Mueller N, van Sintern W, Tschiesner A. Lightweight, heavy impact. 2012 [Accessed 14 November 2018]. 〈https://www.mckinsey.com/~/media/mckinsey/dotcom/client_service/automotive%20and%20assembly/pdfs/lightweight_heavy_impact.ashx〉.

[3] Seidensticker M. COMPOSITESEUROPE 2017: Lightweight automotive construction propels use of fibre-reinforced plastics. 〈http://www.reedexpo.com/de/Pressemitteilungen/2017-Press-Releases/COMPOSITES-EUROPE-2017-Lightweight-automotive-construction-propels-use-of-fibre-reinforced-plastics/〉. [Accessed 14 November 2018]. 2017.

[4] Stewart R. Carbon fibre composites poised for dramatic growth. Reinf Plast 2009;53(4). https://doi.org/10.1016/S0034-3617(09)70148-1.

[5] Schwingenschloegl A, Verghese N, Bruckbauer P, Ehard S, Drechsler K. Towards thermoplastic carbon fiber reinforced plastics for the automotive industry. In: Proceedings of the ECCM17. Munich, Germany, 26–30th June; 2016.

[6] Tenhaeff K, Drechsler K. Hybrid structures of metals and fiber reinforced thermoplastics for chassis components. In: Proceedings of the ECCM17. 2016. Munich, Germany, 26-30th June; 2016.

[7] Erber A, Spitko S. Expanded role for thermoplastic composites. Reinf Plast 2014;58(4). https://doi.org/10.1016/S0034-3617(14)70178-X.

[8] Nishida H, Carvelli V, Fujii T, Okubo K. Thermoplastic vs. thermoset epoxy carbon textile composites. IOP Conf Ser: Mater Sci Eng 2018:406. https://doi.org/10.1088/1757899X/406/1/012043.

[9] Osiecki T, Gerstenberger C, Hackert A, Czech A, Nossol P, Łagoda T. et al. Metal/composite hybrids for lightweight applications. 〈http://mdr.simr.pw.edu.pl/index.php/MDR/article/view/143〉. [Accessed 04 December 2018]; 2015.

[10] Reinhard J, Loehner L-N. Auslegung einer flächigen metall-FVK-Hybridstruktur unter Berücksichtigung der werkstoffspezifischen thermischen Ausdehnungskoeffizienten. Germany: Wolfsburg; 2016. [24–25th May].

[11] Schnurr R, Lippky K, Loechte C, Dietrich F, Droeder K, Kreling S et al. Introduction of a production technology for the pre-assembly of multi-material-preforms aiming at a large scale production. In: Proceedings of the ICCM20, Copenhagen, Denmark, 19–24th July 2015; 2015.

[12] Ghassemieh E. Materials in automotive application, state of the art and prospects. In: Chiaberge M, editor. New trends and developments in automotive industry. London: InTech; 2011.

[13] Hovorun TP, Berladir KV, Pererva VI, Rudenko SG, Martynov AI. Modern materials for automotive industry. JES 2017;4(2). https://doi.org/10.21272/jes.2017.4(2).f8.

[14] Ickert L. FVK-metall-hybridbauweise für die automobile Großserie. Aachen: Forschungsgesellschaft Kraftfahrwesen mbh Aachen; 2013.

[15] Ageorges C, Ye L. Fusion bonding of polymer composites. London: Springer London; 2002.

[16] Huembert M, Mitschang P. Influence of active component cooling on process speed and joint strength during continuous induction joining of glass fiber reinforced polyamide 6 and steel. Mater -Wiss Werkst 2016;47(11). https://doi.org/10.1002/mawe.201600629.

[17] Mitschang P, Velthuis R, Emrich S, Kopnarski M. Induction heated joining of aluminum and carbon fiber reinforced nylon 66. J Thermoplast Compos Mater 2009;22(6). https://doi.org/10.1177/0892705709105969.

[18] Behrens B-A, Huebner S, Neumann A. Forming sheets of metal and fibre-reinforced plastics to hybrid parts in one deep drawing process. Procedia Eng 2014;81. https://doi.org/10.1016/j.proeng.2014.10.198.

[19] Hopmann C, Klein J, Schoenfuss BI, Reisgen U, Schoenberger J, Schiebahn A. Analysis and specification of the crash behaviour of plastics/metal-hybrid composites by experimental and numerical methods. Prod Eng Res Devel 2017;11(2). https://doi.org/10.1007/s11740-017-0727-6.

[20] Hopmann C, Boettcher A, Fischer K. Investigations of bonding approaches and initial bond strength for the intrinsic manufacturing of laminary bonded hybrids made of thermoplastic composite and metal. J Plast Technol 2013;9(6).

[21] Huang C, Wang X, Wu YW, Meng DD, Liu HX. Experimental study of laser direct joining of metal and carbon fiber reinforced nylon. KEM 2014;620. https://doi.org/10.4028/www.scientific.net/KEM.620.42.

[22] Rodríguez-Vidal E, Lambarri J, Soriano C, Sanz C, Verhaeghe G. A combined experimental and numerical approach to the laser joining of hybrid polymer – metal parts. Phys Procedia 2014;56. https://doi.org/10.1016/j.phpro.2014.08.101.

[23] Roesner A, Scheik S, Olowinsky A, Gillner A, Reisgen U, Schleser M. Laser assisted joining of plastic metal hybrids. Phys Procedia 2011;12. https://doi.org/10.1016/j.phpro.2011.03.146.

[24] Heckert A, Zaeh MF. Laser surface pre-treatment of aluminium for hybrid joints with glass fibre reinforced thermoplastics. Phys Procedia 2014;56. https://doi.org/10.1016/j.phpro.2014.08.032.

[25] Goushegir SM, Amancio-Filho ST. Friction spot Joining (FSpJ). In: Amancio S, Blaga L, editors. Joining of polymer-metal hybrid structures: principles and applications. New York: John Wiley et Sons; 2018. p. 61–99.

[26] Goushegir SM. Friction spot joining of metal-composite hybrid structures. Hamburg: TUHH Universitätsbibliothek; 2015.

[27] Bayerl T, Duhovic M, Mitschang P, Bhattacharyya D. The heating of polymer composites by electromagnetic induction – a review. Compos Part A 2014;57. https://doi.org/10.1016/j.compositesa.2013.10.024.

[28] Byskov-Nielsen J, Balling P. Laser structuring of metal surfaces: micro-mechanical interlocking. Appl Surf Sci 2009;255(10). https://doi.org/10.1016/j.apsusc.2008.07.118.

[29] Demir AG, Maressa P, Previtali B. Fibre laser texturing for surface functionalization. Phys Procedia 2013;41. https://doi.org/10.1016/j.phpro.2013.03.145.

[30] Nestler DJ, Döhler C, Wielage B, Wagner G. Surface and fracture surface analysis of thermally bonded metal/FRPjoints. MSF 2015;825–826. https://doi.org/10.4028/www.scientific.net/MSF.825-826.328.

[31] Schuberth A, Goering M, Lindner T, Toeberling G, Puschmann M, Riedel F, et al. Effect of new adhesion promoter and mechanical interlocking on bonding strength in metal-polymer composites. IOP Conf Ser: Mater Sci Eng 2016:118. https://doi.org/10.1088/1757-899x/118/1/012041.

[32] Fuchs AN, Wirth FX, Rinck P, Zaeh MF. Laser-generated macroscopic and microscopic surface structures for the joining of aluminum and thermoplastics using friction press joining. Phys Procedia 2014;56. https://doi.org/10.1016/j.phpro.2014.08.088.

[33] Lippky K, Mund M, Blass D, Dilger K. Investigation of hybrid fusion bonds under varying manufacturing and operating procedures. Compos Struct 2018. https://doi.org/10.1016/j.compstruct.2018.01.078.

[34] Buechter E. A green way to clean - laser cleaning. Laser Technol 2012;9(5). https://doi.org/10.1002/latj.201290068.

[35] van der Straeten K, Burkhardt I, Olowinsky A, Gillner A. Laser-induced self-organizing microstructures on steel for joining with polymers. Phys Procedia 2016;83. https://doi.org/10.1016/j.phpro.2016.08.119.

[36] Huegel H. Strahlwerkzeug laser. Wiesbaden: Vieweg + Teubner Verlag; 1992.

[37] Wirth FX, Fuchs AN, Rinck P, Zaeh MF. Friction press joining of laser-texturized aluminum with fiber reinforced thermoplastics. AMR 2014;966–967. https://doi.org/10.4028/www.scientific.net/AMR.966-967.536.

[38] Rechner R, Jansen I, Beyer E. Laseroberflächenvorbehandlung von aluminium zur optimierung der oxidschichteigenschaften für das strukturelle Kleben. In: DVS-Media, editor. 2. Doktorandenseminar Klebtechnik. Duesseldorf; 2012, p. 1–6.

[39] Pereira A, Delaporte P, Sentis M, Cros A, Marine W, Basillais A, et al. Laser treatment of a steel surface in ambient air. Thin Solid Films 2004;453–454. https://doi.org/10.1016/j.tsf.2003.11.072.

[40] Heckert A, Singer C, Zaeh M. Pulsed laser surface pre - treatment of aluminium to join aluminium pulsed laser surface pre-treatment of aluminium to join aluminium-thermoplastic hybrid parts. 〈https://www.wlt.de/lim/Proceedings/Stick/PDF/Contribution259_final.pdf〉; 2015. [Accessed 14 November 2018].

[41] Brunauer S, Emmett PH, Teller E. Adsorption of gases in multimolecular layers. J Am Chem Soc 1938;60(2). https://doi.org/10.1021/ja01269a023.

[42] Uezuem M. Metal polymer hybrids: multiscale adhesion behaviour and polymer dynamics. Berlin: Technische Universität Berlin; 2015.

[43] Jedlovszky P, Mezei M, Vallauri R. A molecular level explanation of the density maximum of liquid water from computer simulations with a polarizable potential model. Chem Phys Lett 2000;318(1–3). https://doi.org/10.1016/S0009-2614(00)00002-6.

[44] El Sayed A, Eckert A. Dimensions- und Dichteänderung von polymidformteilen durch Wasseraufnahme. Angew Makromol Chem 1991;185(1). https://doi.org/10.1002/apmc.1991.051850106.

[45] Ishisaka A, Kawagoe M. Examination of the time-water content superposition on the dynamic viscoelasticity of moistened polyamide 6 and epoxy. J Appl Polym Sci 2004;93(2). https://doi.org/10.1002/app.20465.

[46] Heym M. Polyamide, polyester und polyoxymethylen. Die klassischen technischen kunststoffe und ihre perspektiven. Angew Makromol Chem 1997;244(1). https://doi.org/10.1002/apmc.1997.052440104.

[47] Velthuis R. Induction welding of fiber reinforced thermoplastic polymer composites to metals. Kaiserslautern: Inst. für Verbundwerkstoffe; 2007.

[48] VDI-Wärmeatlas. Berlin, Heidelberg: Springer Berlin, Heidelberg; 2013.

[49] Winkler HGF. Struktur und eigenschaften der krystalle, Berlin. Heidelberg: Heidelberg: Springer Berlin; 1950.

[50] Goodwin FE. Developments in the production of galvannealed steel for automotive. Trans Indian Inst Met 2013;66(5-6). https://doi.org/10.1007/s12666-013-0290-6.